Journal of The Electrochemical Society

The Electrochemical Society
Advancing solid state & electrochemical science & technology

Electrocatalytic Reduction of Nitrate to Ammonia at Oxidized Vanadium Surfaces with V(3$^+$) and V(4$^+$) Oxidation States

To cite this article: Qasim Adesope *et al* 2024 *J. Electrochem. Soc.* **171** 076504

Journal of The Electrochemical Society, 2024 **171** 076504

Electrocatalytic Reduction of Nitrate to Ammonia at Oxidized Vanadium Surfaces with $V(3^+)$ and $V(4^+)$ Oxidation States

Qasim Adesope,[=] Mohammad K. Altafi,[=] Stella C. Amagbor, Kabirat Balogun, Manan Guragain, Alankar Kafle, Vitaly Mesilov, Francis D'Souza,[*,z] Thomas R. Cundari,[z] and Jeffry A. Kelber[z]

Department of Chemistry, University of North Texas, 305070, Denton, Texas 76203-5017, United States of America

The electrochemical reduction of nitrate to ammonia is of interest as an energy/environmentally friendly source of ammonia for agriculture and energy applications and as a route toward groundwater purification. We report in situ photoemission data, electrochemical results, and density functional theory calculations that demonstrate vanadium oxide—prepared by ambient exposure of V metal, with a distribution of surface V^{3+} and V^{4+} oxidation states—specifically adsorbs and reduces nitrate to ammonia at pH 3.2 at cathodic potentials. Negligible cathodic activity in the absence of NO_3^- indicates high selectivity with respect to non-nitrate reduction processes. In situ photoemission data indicate that nitrate adsorption and reduction to adsorbed NO_2 is a key step in the reduction process. NO_3RR activity is also observed at pH 7, albeit at a much slower rate. The results indicate that intermediate (non-d^0) oxidation states are important for both molecular nitrogen and nitrate reduction to ammonia.
 [DOI: 10.1149/1945-7111/ad60f8]

Manuscript submitted April 14, 2024; revised manuscript received June 1, 2024. Published July 17, 2024.

Supplementary material for this article is available online

The electrocatalytic reduction of nitrate to ammonia (NO_3RR) is of interest, both as a source of NH_3 for agriculture and energy applications and as a route toward water purification from nitrates.[1–4] Pt, Ru, and other noble and semi-precious metals have been demonstrated to be NO_3RR-active.[5–7] The search for Earth-abundant catalysts has examined transition metal-based systems of varying oxophilicities.[1,3] Current research in electrocatalytic nitrate reduction is much more focused on the development of highly active and efficient electrocatalysts; Cu-based materials are attracting tremendous attention due to their outstanding NO_3^- binding affinity.[2,8,9] Similarly, some research with Fe, Co, Ni, Ti, *etc* based catalysts has also been reported, but other potentially promising transition metals such as V, Cr, Mn, *etc* based catalysts have been rarely explored.[10–23] A fundamental understanding of issues governing nitrate-surface interactions and mechanisms remains a relatively sparse but growing area of interest.[5–7,24,25]

Our recent studies of fundament oxide/oxynitride surface interactions relevant to N_2 reduction to NH_3 (NRR) demonstrated that surface metal cations in intermediate (non-d^0) oxidation states are essential for NRR, indicating the dominant role that metal d-to-N_2 π^* backbonding plays in N_2 binding and N≡N bond activation.[26–29] An important and intriguing question is whether such NRR-active Earth-abundant oxide surfaces can also bind and activate NO_3^- as an alternative to Pt, Ru, *etc.*

We focus here on vanadium oxide, a system we have previously characterized by experiments and theory and demonstrated to be a highly selective and active catalyst for NRR.[26,27,30] Experimental and theoretical studies[27,29] indicate that the V^{3+} oxidation state most strongly binds N_2 (vs H_2O) at V surface sites and activates N≡N bonds for H+/e- transfer due to V 3d to N_2 π^* backbonding. The experimental and theoretical results described herein indicate that similar systems enhance nitrate (and nitrite)/vanadium oxide bonding and N-O bond activation, suggesting that Earth-abundant metal suboxides with surface cations in intermediate (non-d^0) oxidation states under electro-reduction conditions are active for both NRR and NO_3RR. The present findings represent the first in situ photoelectron spectroscopic study of specific nitrate absorption and reduction to ammonia at a cathodic surface under NO_3RR conditions.

Experimental Methods

Sample deposition and surface analysis.—Vanadium thin films were deposited by direct current (DC) magnetron sputter deposition in a system with sputter deposition and in situ Auger electron spectroscopy (AES) capability as described previously,[30] from a commercial V sputter target (99.7% purity, Plasmaterials) at a base pressure of 10^{-8} Torr. Films were deposited on commercially available fluorinated tin oxide (FTO) substrates at room temperature. Although the present film thicknesses were not measured directly, previous experiments using similar deposition parameters yielded ~500 Å thick films.[30] In situ sample transfer to the adjacent AES chamber was accomplished without exposure to ambient. AES spectra were acquired using a commercial single-pass cylindrical mirror analyzer (ESA 100, STAIB Instruments) with a concentric electron gun operating at 3 keV. Next, the deposited film was transferred in ambient to another chamber for X-ray photoelectron spectroscopy (XPS) analysis. XPS spectra were acquired on the ambient exposed sample and then subjected to Ar ion sputtering (3 keV) to remove C and N contaminants from the surface. XPS spectra were acquired in a system equipped with a Physical Electronics (PHI) 140 mm mean radius hemispherical analyzer with micro-channel plate detector operated in the constant pass energy mode (23 eV). Unmonochromatized Al Kα X-rays were used, obtained from a PHI 04–548 dual anode X-ray source, operated at 15 KeV, 300 W. Analysis of XPS data was carried out by standard methods.[31] Peak fitting employed Gaussian–Lorentzian components and was carried out as described previously.[30,32] XPS binding energies were calibrated to an O1s peak maximum of 530.0 eV for lattice oxygen.[33] To probe surface changes upon electrochemical (EC) study, XPS measurements involving in situ sample transfer between ultra-high vacuum (UHV) and EC environments were performed using the system described previously.[34] In brief, this UHV-EC system comprised of an antechamber and a UHV chamber equipped with EC cell and XPS capability respectively. The antechamber and UHV chambers were separated by a gate valve and their pressures were maintained at 10^{-6} and 10^{-9} Torr, respectively, using different turbomolecular pumps. The sample was loaded on the system through the introduction chamber and the transfer arm was used to move the sample to the UHV

[=]Equal Contribution.
*Electrochemical Society Fellow.
[z]E-mail: Francis.DSouza@UNT.edu; Thomas.Cundari@unt.edu; Jeffry.Kelber@unt.edu

chamber where XPS analysis was done prior to EC studies. After XPS, the sample was transferred to the antechamber for EC measurement. Prior to EC experiments, the antechamber was back-filled with Ar gas to bring its pressure to 23.7 Torr (corresponds to ambient pressure) after which the EC cell was introduced into the chamber by the opening of a gate valve separating them. After each immersion in electrolyte, the sample was rinsed in Ar-purged Millipore water and the EC cell was lowered out of the antechamber for proper isolation between it and the cell. The antechamber was pumped back to 10^{-6} Torr, and the sample was moved from the antechamber to the UHV for in situ XPS characterization.[30,34]

***Electrochemical studies.*—**All EC studies, including linear scan voltammetry (LSV) and chronoamperometry (CA), were carried out using an EG&G 263 potentiostat by employing the V-coated FTO glass as working electrode with platinum wire and Ag/AgCl as counter and reference electrodes respectively. The LSV study was carried out in a single-compartment cell, whereas the CA study for bulk electrolysis was performed in a two-compartment H-type cell separated by a Nafion membrane. The electrolytes were purged with argon gas before electrochemical measurements.

The amount of NH_3 formed during electrolysis was estimated spectrophotometrically with the indophenol blue method by using a JASCO V-670 ultraviolet-visible (UV–vis) spectrophotometer. After the bulk electrolysis, 2 mL of electrolyte was taken out and 2 mL alkaline solution containing mixture of salicylic acid and trisodium citrate (5% each in 1 M KOH) followed by 1 ml sodium hypochloride (0.05 M) and 200 μl of sodium nitroprusside solution (1%) were added on it and left for 1.5 h for color development. Finally, a spectrophotometric spectrum was recorded under wavelength range of 500–750 nm and amount of NH_3 formed was determined.[35]

The Faradic efficiency (FE) for ammonia formation was estimated by using the following formula:

$$FE(\%) = \frac{8 \times C_{NH3} \times F \times V}{17 \times Q} \times 100$$

where F is the Faraday constant, C_{NH3} is the amount of NH_3 quantified, V is the volume of electrolyte and Q is the amount of charge supplied during the electrolysis.

The intermediate nitrite (NO_2^-) was quantified spectrophotometrically, for which, series of nitrite standard solutions with different concentrations, i.e., 2 to 100 $\mu g\, l^{-1}$ were prepared by using $NaNO_2$ stock solution. For the color development, two reagents—sulphanilamide (0.5 g of sulphanilamide in 50 mL of 2 M HCl) and NEDA (20 mg of N-(1-Napthyl) ethylenediamine dihydrocholoride in 20 mL of deionized H_2O)—were prepared separately. At first, 0.1 ml of sulphanilamide solution was added to the 5 ml of analyte solution and allowed to stand for 10 min. Thereafter, 0.1 ml of NEDA solution was added and kept for 30 min respectively. A spectrum was recorded under wavelength range of 440–600 nm and amount of NO_2^- was estimated.[19]

The FE for nitrite formation was determined by using the following formula:[4]

$$FE(\%) = \frac{2 \times C_{NO2-} \times F \times V}{46 \times Q} \times 100$$

Computational Methods

Plane-wave density functional theory (DFT) computations utilized the Vienna *Ab initio* Simulation Package (VASP) version 5.4.4.[36] Van der Waals and continuum solvation corrections were included in the reported simulations.[37] Calculations utilized a plane wave cutoff energy of 500 eV; self-consistent field (SCF) convergence was $<1 \times 10^{-5}$ eV. Surface calculations were done in an asymmetrical unit cell of $a = b = 8.79$ Å, $c = 33.16$ Å, $\alpha = \beta = \gamma = 90°$, and used a K-point mesh of $3 \times 3 \times 1$. Calculations utilized 1st-order Methfessel–Paxton smearing with $\sigma = 0.2$ eV.[38] Simulations utilized spin-polarized methods, with projector-augmented wave (PAW) potentials and generalized gradient approximation (GGA) functionals.[37] DFT-D3 van der Waals corrections[39] with Becke-Johnson[40] damping were included in the simulations. The XPS spectra calculations of N1s and O1s core energies were carried out using optimized geometries of adsorbates and the adsorbate-free rutile VO_2 (111) surface only. In these calculations, the final-state approximation and the K-point integration mesh of $7 \times 7 \times 1$ were used.

Results and Discussion

Catalyst thin film electrodes were prepared by DC magnetron sputter deposition of V metal onto FTO, which was subsequently exposed to the ambient to form the oxide film. In situ AES and ex situ XPS spectra after such exposure indicated no observable N surface concentration, with an average V oxidation state (proportional to the $V2p_{3/2}$—O1s binding energy difference[27,41]) close to 4+ (Figs. S1 and S2). The V oxide films were subjected to EC measurements in three different electrolytes: (i) 0.1 M $NaNO_3$ adjusted to pH 3.2 with HNO_3, (ii) 0.1 M Na_2SO_4 adjusted to pH 3.2 with H_2SO_4, and (iii) 0.1 M $NaNO_3$ (pH 7). V oxide formed by ambient exposure is NRR active and HER inactive at pH 7.[28,30] The pH of the electrolyte was measured before and after electrolysis for 1.5 h. No significant change in pH ($\delta \sim 0.1$ unit) was observed, which implied that local pH remained approximately the same for the term of electrolysis. Linear scan voltammograms (LSVs) (Fig. 1a) show that the V oxide catalyst in the nitrate-free solution displays a very small increment in cathodic current relative to that of the FTO substrate. In contrast, in nitrate-containing solution (Fig. 1a, a significant cathodic current is displayed at voltages more negative than −0.5 V vs Ag/AgCl. Corresponding indophenol blue absorption measurements are shown in Fig. 1b (see also Fig. S3) after electrolysis in nitrate-containing and nitrate-free solutions at −0.85 and −0.75 V vs Ag/AgCl, respectively, for 1.5 h. The significant absorption (Fig. 1b) observed upon electrolysis in nitrate-containing solution confirms the formation of NH_3, with a FE of 25% and yield rate of 890 μmole h^{-1} g_{cat}^{-1}, a robust value for a low surface area 2D film surface. Indeed, while similar FE values have been observed for NRR with vanadium oxide or oxynitride thin films,[30,42] these materials display far higher FEs in practical, high surface area form and are among the most promising for NRR applications.[43] However, the significant increment of cathodic current in the presence of sodium nitrate at pH 3.2 compared to Na_2SO_4 electrolyte at similar pH (Fig. 1a) is not justifiable with the observed FE value for ammonia formation alone. Therefore, another possible intermediate, the nitrite ion (NO_2^-), was estimated spectrophotometrically. A high absorbance observed around 540 nm (Fig. S4) with an FE of 9.9% evidenced the formation of nitrite as an intermediate product, which was not converted to ammonia as a final product at the applied potential of −0.85 V vs Ag/AgCl. A trace amount of hydroxylamine (FE < 0.05%, by the *o*-phenanthroline method) was found, but neither hydrazine (via the Watt-Chrisp test) nor H_2 via GC was observed. These findings suggest the formation of other non-NH_3 nitrogen-containing reaction products.

At pH 7, despite the low cathodic current (Fig. 1a), the calculated NH_3 FE is found to be 2.74%, due to the small amount of charge passed. Corresponding data in nitrate-free solution at pH 3.2 (Fig. 1b) show only background absorbance, indicating no NH_3 was produced. Thus, the data in Fig. 1 demonstrate that V oxide formed by ambient exposure of V metal is NO_3RR-active at pH 3.2, at potentials more negative than −0.5 V vs Ag/AgCl. Similar NO_3RR behavior is observed at pH 7 but with a much lower rate of NH_3 formation. The reduced increment of cathodic current in nitrate-free solution at pH 3.2 (Fig. 1a) compared to nitrate-containing solution strongly suggests that the V oxide is much more selective for NO_3RR concerning the HER under these conditions, consistent

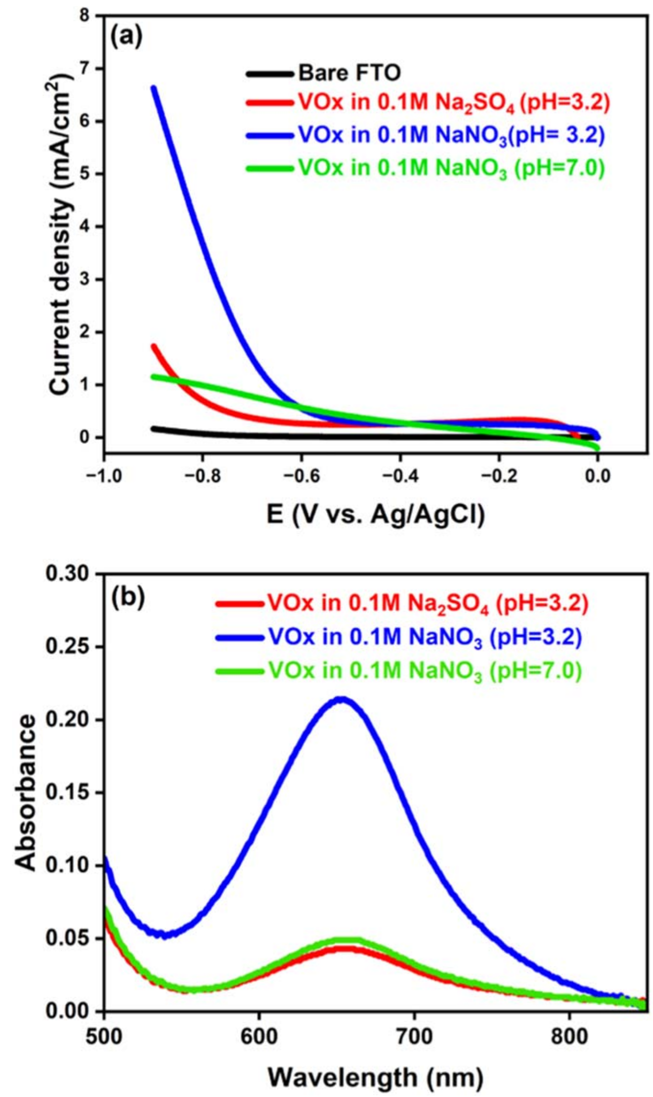

Figure 1. Electrochemical data: (a) Linear scan voltammograms for VO_x catalysts in nitrate and nitrate-free solutions at pH 3.2; and in 0.1 M Na_2NO_3 (pH 7). (b) Indophenol blue absorption spectrum developed using electrocatalytically produced NH_3 for VO_x electrode in nitrate solution after electrolysis for 1.5 h at −0.85 V vs Ag/AgCl in 0.1 M $NaNO_3/HNO_3$ (blue curve), and at −0.75 V vs Ag/AgCl in 0.1 M Na_2SO_4/H_2SO_4 n (red curve) and 0.1 M $NaNO_3$ (green curve).

with GCMS results mentioned above. Electrochemical nitrate reduction involves the adsorption of nitrate species over the electrode surface, followed by hydrogenation. At acidic pH, the protons present in the electrolyte provide the hydrogen needed for hydrogenation, whereas adsorbed hydrogen is the source of hydrogen for hydrogenation at neutral pH conditions.[2] From the LSVs and electrolysis product analysis results (Fig. 1), it is inferred that solution protons are more beneficial for hydrogenation of the adsorbed nitrate species during electrolysis vs adsorbed hydrogen species, thus resulting in higher activity towards nitrate reduction in acidic vs neutral pH. Previous studies[28] have established that V oxynitrides are also inactive for HER vs NRR at 0.1 M Na_2SO_4 (pH 7).

In situ photoemission studies involving controlled sample transport between EC and UHV environments were carried out on the V oxide catalysts to (i) determine the nature of the V oxide surface and the specific adsorption of nitrate anions from solution on that surface at open circuit potential (OCP) at pH 3.2, and (ii) examine the evolution of the surface oxide and adsorbates upon polarization to more cathodic potentials. Those measurements were carried out in a nitrate-free (0.1 M Na_2SO_4/H_2SO_4) solution to avoid further specific nitrate adsorption confusing the results at more cathodic potentials. A potential of −1.0 V vs Ag/AgCl was selected for UHV-EC measurements to determine the effects on nitrate oxidation states and surface concentration under maximal practical reduction conditions. The results are displayed in Fig. 2. XPS binding energies were calibrated with the O1s peak maximum at 530 eV (Figs. 2a–2c) for lattice O, in agreement with previous studies of V oxide surfaces,[11,25] and other transition metal oxide surfaces.[33,44,45]

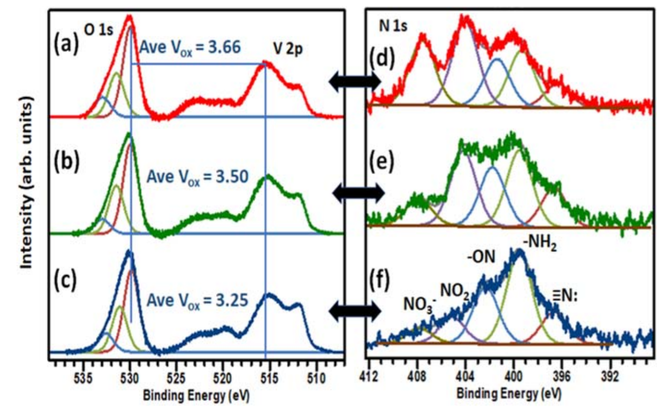

Figure 2. UHV-EC results for ambient-exposed V sample. (a) O1s/V2p spectra upon immersion/emersion at OCP in 0.1 M $NaNO_3/HNO_3$ (pH 3.2), rinsing in DI water, and transfer to UHV for XPS. (b) Subsequent immersion at OCP and polarization to −0.5 V vs Ag/AgCl in nitrate-free 0.1 M Na_2SO_4/H_2SO_4 solution (pH 3.2) and emersion/rinsing at that potential. (c) O1s/V2p spectra upon immersion in nitrate-free pH 3.2 solution at OCP and emersion at -1.0 V vs Ag/AgCl. (d)–(f) are corresponding N1s spectra for (a)–(c) respectively. The average V oxidation state is proportional to the difference between O1s and V2p peak binding energies (Refs. 11 and 15). Peak assignments for the N1s spectra (f) are based on literature precedents and DFT calculations.

The decomposition of the V2p XPS spectrum is complex.[41] Thus, the data in Figs. 2a–2c display the average V oxidation state.[27,41] Although the average V oxidation state is ∼4+ before immersion (Fig. S2), immersion at OCP yields a significant reduction in oxidation state, consistent with the Pourbaix diagram,[46] with further reduction upon cathodic polarization. UHV-EC experiments indicate the V oxide surface exhibits predominantly V^{4+} and V^{3+} oxidation states, with the latter predominant at more cathodic potentials.

N1s spectra (Figs. 2d–2f) are similar to those observed upon exposure of Fe_2O_3 to HNO_3 vapor and subsequent reaction with water vapor, O_2, and UV radiation.[44] The N1s feature near 407 eV binding energy (Fig. 2d) is assigned to adsorbed nitrate (NO_3^-).[44,45] Our DFT calculations (Table S1) also assign the feature near 406 eV (Fig. 2f) to adsorbed NO_2, *viz* N in a 4+ formal oxidation state, in good agreement with previous studies. Similarly, our assignment of the N1s feature near 402 eV (Fig. 2f) to NO is in good agreement with previous studies.[29] The assignments (Fig. 2f) of the features near 400 eV and 396.5 eV to V = NH and to V≡N:, respectively, agree with previous studies of V oxynitrides.[47,48]

The data in Figs. 2d–2f are scaled to the intensity of the O1s feature at 530 eV, so the N1s intensities are directly comparable. These data thus show that the cathodic polarization of the V oxide electrode results in the reduction of highly oxidized N features, leaving only adsorbed N species in reduced nitrogen oxidation states. Importantly, as the N1s spectra in Figs. 2e, 2f were acquired in *nitrate-free* solutions, the XPS data demonstrate that the nitrate species specifically adsorbed at OCP are reacting. Hence, the N1s spectra (Figs. 2d, 2f) demonstrate the reduction of specifically adsorbed oxidized N species, beginning at potentials near −0.5 eV vs Ag/AgCl, in very good agreement with the LSV data (Fig. 1a) and electrolysis product analysis (Figs. 1b, S3–4).

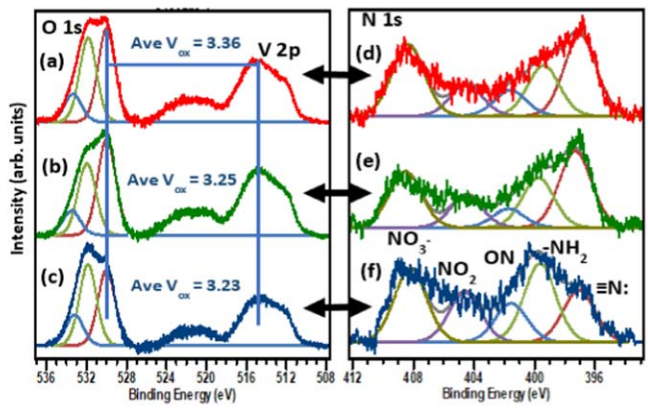

Figure 3. UHV-EC results for ambient-exposed V sample. (a) O1s/V2p spectra upon immersion/emersion at OCP in 0.1 M $NaNO_3$ (pH 7), rinsing in DI water, and transfer to UHV for XPS. (b) Subsequent immersion at OCP and polarization to -0.5 V vs Ag/AgCl in nitrate free 0.1 M Na_2SO_4 solution (pH 7) and emersion/rinsing at that potential. (c) O1s/V2p spectra upon immersion in nitrate-free pH 7 solution at OCP and emersion at -1.0 V vs Ag/AgCl. (d)–(f) are corresponding N1s spectra for (a)–(c) respectively. The average V oxidation state is proportional to the difference between O1s and V2p peak binding energies (*cf* Refs. 6 and 10). Peak assignments for the N1s spectra (f) are based on literature precedents and DFT calculations.

Figure 3 displays XPS binding energy calibrated to O1s at 530 eV corresponding to lattice O. The V2p XPS spectra are expressed in average oxidation state as previously reported.[27,41] UHV-EC experiments indicate that the V oxide surface region displays oxidation states of both V^{4+} and V^{3+}, but becomes predominately V^{3+} upon polarization to more cathodic potential. The observed N1s spectra (Figs. 3d–3f) are like that previously reported when Fe_2O_3 is exposed to HNO_3 vapor and further reacted with O_2 and UV radiation.[33,44,45] After immersion at OCP, N1s (Figs. 2, 3d) showed sufficient adsorption of a highly oxidized N feature depicted as the nitrate (NO_3^-) component at binding energy ∼407 eV for both acidic and neutral pH (3.2 and 7). The above data showed a slight reduction in the highly oxidized N feature after cathodic polarization to -0.5 V in 0.1 M Na_2SO_4 -nitrate-free solution at pH 7, which correlates with the slight ammonia formation observed in the absorption spectrum (Fig. 1b) at pH 7. However, cathodic polarization to -0.5 V in the same electrolyte at pH 3.2 significantly reduced the nitrate feature. Further polarization to -1.0 V showed no significant reduction in the highly oxidized N feature at pH 7, but polarization at pH 3.2 shows a subsequent decrease in this feature. Therefore, N1s spectra (Figs. 3e, 3f) signify no significant reduction of adsorbed oxidized N species, beginning at potentials of ca. -0.5 V vs Ag/AgCl or more at pH 7, which corroborates the LSV (Fig. 1a) and absorption spectrum (Fig. 1b) data. While at pH 3.2, N1s spectra indicate a significant reduction in absorbed oxidized species beginning at -0.5 V vs Ag/AgCl and more cathodic potentials (Figs. 2e, 2f), also in good agreement with the LSV (Fig. 1a) and absorption spectrum data. The results indicate sufficient proton availability at pH 3.2 to reduce adsorbed nitrate to NH_3, thus generating an FE of 25%. In contrast, at pH 7, there is insufficient proton concentration to reduce nitrate to ammonia, leaving the adsorbed nitrate feature intense after polarization and yielding an FE of only 2.7%.

In a significant recent paper, Carvalho et al.[49] indicated that nitrite binding strength and facile *NO dissociation to *N and *O as key factors in NO_3RR catalysis by transition metals. These findings are consistent with our results indicating some nitrite formation during NO_3RR and point to the importance of d-to-π back-bonding.

A priori, one may have expected anions would prefer ligation to more Lewis acidic vanadyl (4+) vs vanadous (3+) ions. However, our DFT calculations for several model surfaces of V oxide (V_2O_5) vs suboxides (Fig. 4, Table S2) indicate that *nitrate and nitrite both bind more strongly to* V^{3+} *than* V^{4+}*suboxide sites and binding to* V^{5+} *is negligible*. Computations also indicate that the formal oxidation state of the metal—primarily—and coordination number of the surface vanadium site—secondarily - play a strong role in nitrite and nitrate binding efficiency. For example, modeling three V^{4+} surface models shows that nitrite bonding is distinctly impacted by metal coordination number: rutile-VO_2(110) = -1.2 eV (octahedral), rutile-VO_2(110) = -1.9 eV (square pyramid), and C_{2m}-VO_2(100) = -3.3 eV (trigonal planar). Similar trends are seen in nitric oxide, nitric acid, etc, binding energies (Table S2).

Regarding the ability to bind and activate adsorbed nitrosyl (*NO), metal sites with lower formal oxidation states that are more coordinatively unsaturated more strongly bind and activate NO. For example, NO binding to the surface V^{5+} sites of V_2O_5(010) is weak ($\Delta E = -0.1$ eV), while binding to V^{3+} surface sites is much more favorable ($\Delta E = -3.2$ eV for R_{3c}-V_2O_3(0001)); for the V^{4+} models the energetics are intermediate these two extremes, being enhanced by a reduced vanadium coordination number (Table S2). NO scission to *O + *N is also increasingly energetically favored as the surface V sites are reduced in formal oxidation state and coordination number. Our computational results thus corroborate the importance of V^{4+}/V^{3+} sites in the NO_3RR process.

In summary, the electrochemical (Fig. 1 and in situ photoemission (Fig. 2) results presented here demonstrate that V oxide electrocatalysts formed by ambient exposure of V metal are NO_3RR-active at pH 3.2, with an FE of 25%—quite high for a low surface-area film.[30,42] The XPS spectra (Fig. 2) also indicate that the active surface consists of predominantly V^{3+} and some V^{4+} sites, in agreement with theory (Fig. 4, Table S1), indicating that V^{3+} surface sites are energetically preferred for nitrate and nitrite binding and NO dissociation**.** These results are consistent with recent findings[49] and demonstrate the key role of d/π back-bonding in the NO_3RR process.

These results further suggest that the broad concepts regarding nitrate catalysis and periodic trends recently proposed for metals[49] may extend beyond transition metals to the corresponding oxides.

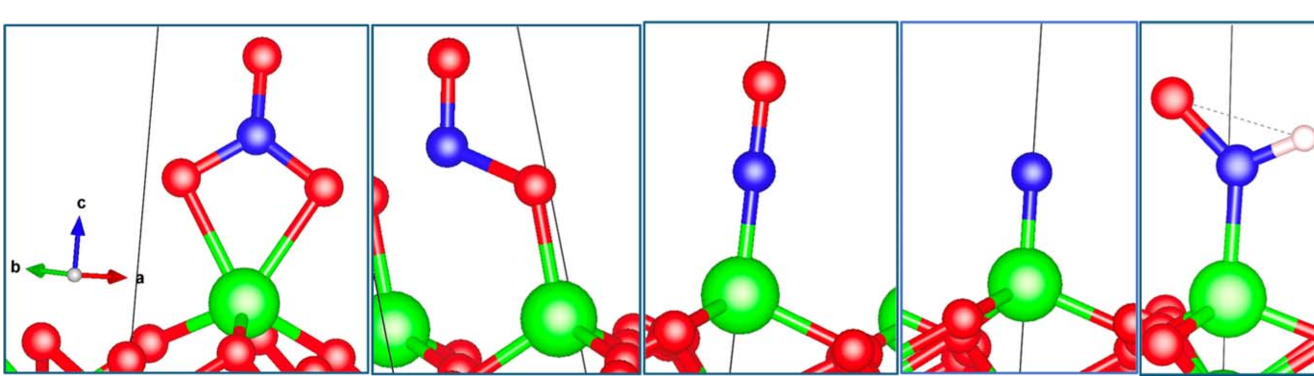

Figure 4. Important surface intermediates in nitrate reduction on R_{3c}-V_2O_3(0001), from left to right: κ^2-nitrate, κ^1-O-nitrite, κ^1-N-nitrosyl, terminal nitride, κ^1-N-nitroxyl. Red, blue, and green spheres are oxygen, nitrogen, and vanadium, respectively.

Finally, the demonstrated importance of surface cations in intermediate oxidation states indicates that transition metal oxides that are NRR active should also be NO_3RR active. Importantly, in contrast to PtRu and other semi-noble NO_3RR catalysts,[5] V oxide is inactive for HER at both acidic (*vide supra*) and neutral pH,[28] and as predicted by our DFT calculations.[28]

Important aspects—including the possible formation of other reaction products at various pH values and the effects of pH on effective oxide surface charge and oxidation state distribution, are beyond the scope of this research. Still, future experiments and calculations regarding these issues are in progress in our laboratories. The results herein, however, demonstrate that certain Earth-abundant transition metal oxides—if stabilized in intermediate oxidation states—can be selective catalysts for a variety of electroreduction reactions in which d-to-π^* backbonding plays an important role, including NRR, NO_3RR and, possibly, CO_2RR.

Acknowledgments

This work was supported by the US National Science Foundation under grant DMR-2112864. We also gratefully acknowledge additional NSF support for the UNT CASCaM HPC cluster via grants CHE-1531468 and OAC-2117247.

ORCID

Vitaly Mesilov https://orcid.org/0000-0002-1084-2725
Francis D'Souza https://orcid.org/0000-0003-3815-8949

References

1. X. Liang, H. Zhu, X. Yang, S. Xue, Z. Liang, X. Ren, A. Liu, and G. Wu, "Recent advances in designing efficient electrocatalysts for electrochemical nitrate reduction to ammonia." *Small Struct.*, **4**, 2200202 (2023).
2. X. Lu, H. Song, J. Cai, and S. Lu, "Recent development of electrochemical nitrate reduction to ammonia: A mini-review." *Electrochem. Commun.*, **129**, 107094 (2021).
3. J. M. McEnaney, S. J. Blair, A. C. Nielander, J. A. Schwalbe, D. M. Koshy, M. Cargnello, and T. F. Jaramillo, "Electrolyte engineering for efficient electrochemical nitrate reduction to ammonia on a titanium electrode." *ACS Sustain Chem. Eng.*, **8**, 2672 (2020).
4. Z.-Y. Wu, M. Karamad, X. Yong, Q. Huang, D. A. Cullen, P. Zhu, C. Xia, Q. Xiao, M. Shakouri, and F.-Y. Chen, "Electrochemical ammonia synthesis via nitrate reduction on Fe single atom catalyst." *Nat. Commun.*, **12**, 2870 (2021).
5. G. Dima, A. De Vooys, and M. Koper, "Electrocatalytic reduction of nitrate at low concentration on coinage and transition-metal electrodes in acid solutions." *J. Electroanal. Chem.*, **554**, 15 (2023).
6. Z. Wang, S. D. Young, B. R. Goldsmith, and N. Singh, "Increasing electrocatalytic nitrate reduction activity by controlling adsorption through PtRu alloying." *J. Catal.*, **395**, 143 (2021).
7. J.-X. Liu, D. Richards, N. Singh, and B. R. Goldsmith, "Activity and selectivity trends in electrocatalytic nitrate reduction on transition metals." *ACS Catal.*, **9**, 7052 (2019).
8. Y. Zeng, C. Priest, G. Wang, and G. Wu, "Restoring the nitrogen cycle by electrochemical reduction of nitrate: progress and prospects." *Small Methods*, **4**, 2000672 (2020).
9. J. Martínez, A. Ortiz, and I. Ortiz, "State-of-the-art and perspectives of the catalytic and electrocatalytic reduction of aqueous nitrates." *Appl. Catal. B Environ.*, **207**, 42 (2017).
10. K. Fan, W. Xie, J. Li, Y. Sun, P. Xu, Y. Tang, Z. Li, and M. Shao, "Active hydrogen boosts electrochemical nitrate reduction to ammonia." *Nat. Commun.*, **13**, 7958 (2022).
11. J. Zhang, W. He, T. Quast, J. R. Junqueira, S. Saddeler, S. Schulz, and W. Schuhmann, "Single-entity electrochemistry unveils dynamic transformation during tandem catalysis of Cu_2O and Co_3O_4 for converting NO3− to NH3." *Angew. Chem. Int. Ed.*, **62**, e202214830 (2023).
12. S. Ye, Z. Chen, G. Zhang, W. Chen, C. Peng, X. Yang, L. Zheng, Y. Li, X. Ren, and H. Cao, "Elucidating the activity, mechanism and application of selective electrosynthesis of ammonia from nitrate on cobalt phosphide." *Energy Environ. Sci.*, **15**, 760 (2022).
13. Z. Li, G. Wen, J. Liang, T. Li, Y. Luo, Q. Kong, X. Shi, A. M. Asiri, Q. Liu, and X. Sun, "High-efficiency nitrate electroreduction to ammonia on electrodeposited cobalt–phosphorus alloy film." *Chem. Commun.*, **57**, 9720 (2021).
14. D. Liu, L. Qiao, Y. Chen, P. Zhou, J. Feng, C. C. Leong, K. W. Ng, S. Peng, S. Wang, and W. F. Ip, "Electrocatalytic reduction of nitrate to ammonia on low-cost manganese-incorporated Co_3O_4 nanotubes." *Appl. Catal. B Environ.*, **324**, 122293 (2023).
15. N. C. Kani, N. H.-L. Nguyen, K. Markel, R. R. Bhawnani, B. Shindel, K. Sharma, S. Kim, V. P. Dravid, V. Berry, and J. A. Gauthier, "Electrochemical reduction of nitrates on CoO nanoclusters-functionalized graphene with highest mass activity and nearly 100% selectivity to ammonia." *Adv. Energy Mater.*, **13**, 2204236 (2023).
16. J. Li, M. Li, N. An, S. Zhang, Q. Song, Y. Yang, J. Li, and X. Liu, "Boosted ammonium production by single cobalt atom catalysts with high Faradic efficiencies." *Proc. Natl Acad. Sci.*, **119**, e2123450119 (2022).
17. Y. Yu, C. Wang, Y. Yu, Y. Wang, and B. Zhang, "Promoting selective electroreduction of nitrates to ammonia over electron-deficient Co modulated by rectifying Schottky contacts." *Sci. China Chem.*, **63**, 1469 (2020).
18. Y. Wang, Y. Yu, R. Jia, C. Zhang, and B. Zhang, "Electrochemical synthesis of nitric acid from air and ammonia through waste utilization." *Natl Sci. Rev.*, **6**, 730 (2019).
19. Z. Niu, S. Fan, X. Li, Z. Liu, J. Wang, J. Duan, M. O. Tade, and S. Liu, "Facile tailoring of the electronic structure and the d-band center of copper-doped cobaltate for efficient nitrate electrochemical hydrogenation." *ACS Appl. Mater. Interfaces*, **14**, 35477 (2022).
20. Z. N. Zhang, Q. L. Hong, X. H. Wang, H. Huang, S. N. Li, and Y. Chen, "Au nanowires decorated ultrathin Co_3O_4 nanosheets toward light-enhanced nitrate electroreduction." *Small*, **19**, 2300530 (2023).
21. J. Wang, C. Cai, Y. Wang, X. Yang, D. Wu, Y. Zhu, M. Li, M. Gu, and M. Shao, "Electrocatalytic reduction of nitrate to ammonia on low-cost ultrathin CoO_x nanosheets." *ACS Catal.*, **11**, 15135 (2021).
22. J. Gao, B. Jiang, C. Ni, Y. Qi, Y. Zhang, N. Oturan, and M. A. Oturan, "Non-precious Co_3O_4-TiO_2/Ti cathode based electrocatalytic nitrate reduction: preparation, performance and mechanism." *Appl. Catal. B Environ.*, **254**, 391 (2022).
23. J. Gao, B. Jiang, C. Ni, Y. Qi, and X. Bi, "Enhanced reduction of nitrate by noble metal-free electrocatalysis on P doped three-dimensional Co_3O_4 cathode: mechanism exploration from both experimental and DFT studies." *Chem. Eng. J.*, **382**, 123034 (2020).
24. M. Duca and M. T. Koper, "Powering denitrification: the perspectives of electrocatalytic nitrate reduction." *Energy Environ. Sci.*, **5**, 9726 (2012).
25. Y. Wang, A. Xu, Z. Wang, L. Huang, J. Li, F. Li, J. Wicks, M. Luo, D.-H. Nam, and C.-S. Tan, "Enhanced nitrate-to-ammonia activity on copper–nickel alloys via tuning of intermediate adsorption." *J. Am. Chem. Soc.*, **142**, 5702 (2020).
26. A. Ganesan, A. Osonkie, P. Chukwunenye, I. Rashed, T. R. Cundari, F. D'Souza, and J. A. Kelber, "Communication—Electrochemical reduction of N_2 to ammonia by vanadium oxide thin films at neutral pH: Oxophilicity and the NRR reaction." *J. Electrochem. Soc.*, **168**, 026504 (2021).
27. K. Balogun, P. Chukwunenye, F. Anwar, A. Ganesan, Q. Adesope, D. Willadsen, S. Nemšák, T. Cundari, P. Bagus, and F. D'Souza, "Interaction of molecular nitrogen with vanadium oxide in the absence and presence of water vapor at room temperature: Near-ambient pressure XPS." *J. Chem. Phys.*, **157**, 104701 (2022).
28. P. Chukwunenye, A. Ganesan, M. Gharaee, K. Balogun, F. Anwar, Q. Adesope, T. R. Cundari, F. D'Souza, and J. A. Kelber, "Electrocatalytic selectivity for nitrogen reduction vs hydrogen evolution: a comparison of vanadium and cobalt oxynitrides at different pH values." *J. Mater. Chem. A*, **10**, 21401 (2022).
29. K. Balogun, A. Ganesan, P. Chukwunenye, M. Gharaee, Q. Adesope, S. Nemšák, P. S. Bagus, T. R. Cundari, F. D'Souza, and J. A. Kelber, "Vanadium oxide, vanadium oxynitride, and cobalt oxynitride as electrocatalysts for the nitrogen reduction reaction: a review of recent developments." *J. Phys. Condens. Matter*, **35**, 333002 (2023).
30. A. Osonkie, A. Ganesan, P. Chukwunenye, F. Anwar, K. Balogun, M. Gharaee, I. Rashed, T. R. Cundari, F. D'Souza, and J. A. Kelber, "Electrocatalytic reduction of nitrogen to ammonia: the roles of lattice O and N in reduction at vanadium oxynitride surfaces." *ACS Appl. Mater. Interfaces*, **14**, 531 (2021).
31. M. P. Seah and D. Briggs, *Practical Surface Analysis: Auger and X-ray Photoelectron Spectroscopy*, vol. 1, (1983), Wiley, 1996.
32. A. Osonkie, V. Lee, A. Oyelade, M. Mrozek-McCourt, P. Chukwunenye, T. D. Golden, T. R. Cundari, and J. A. Kelber, "Chemical and electronic structures of cobalt oxynitride films deposited by NH_3 vs N_2 plasma: theory vs experiment." *Phys. Chem. Chem. Phys.*, **22**, 24640 (2020).
33. M. C. Biesinger, B. P. Payne, A. P. Grosvenor, L. W. Lau, A. R. Gerson, and R. S.-C. Smart, "Resolving surface chemical states in XPS analysis of first row transition metals, oxides and hydroxides: Cr, Mn, Fe, Co and Ni." *Appl. Surf. Sci.*, **257**, 2717 (2011).
34. J. Kelber and G. Seshadri, "Adsorbate-catalyzed anodic dissolution and oxidation at surfaces in aqueous solutions." *Surf. Interface Anal.*, **31**, 431 (2001).
35. D. Gupta, A. Kafle, S. Kaur, T. S Thomas, D. Mandal, and T. C. Nagaiah, "Selective electrochemical conversion of N_2 to NH_3 in neutral media using B, N-containing carbon with a nanotubular morphology." *ACS Appl. Mater. Interfaces*, **15**, 4033 (2023).
36. J. Hafner, "Ab-initio simulations of materials using VASP: Density-functional theory and beyond." *J. Comput. Chem.*, **29**, 2044 (2008).
37. G. Kresse and D. Joubert, "From ultrasoft pseudopotentials to the projector augmented-wave method." *Phys. Rev. B*, **59**, 1758 (1999).
38. M. Methfessel and A. Paxton, "High-precision sampling for Brillouin-zone integration in metals." *Phys. Rev. B*, **40**, 3616 (1989).
39. S. Grimme, J. Antony, S. Ehrlich, and H. Krieg, "A consistent and accurate *ab initio* parametrization of density functional dispersion correction (DFT-D) for the 94 elements H-Pu." *J. Chem. Phys.*, **132**, 154104 (2010).
40. A. D. Becke and E. R. Johnson, "Exchange-hole dipole moment and the dispersion interaction: High-order dispersion coefficients." *J. Chem. Phys.*, **124**, 014104 (2006).
41. D. Goodacre, M. Blum, C. Buechner, H. Hoek, S. M. Gericke, V. Jovic, J. B. Franklin, S. Kittiwatanakul, T. Söhnel, and H. Bluhm, "Water adsorption on vanadium oxide thin films in ambient relative humidity." *J. Chem. Phys.*, **152**, 044715 (2020).

42. P. Chukwunenye, A. Ganesan, M. Gharaee, K. Balogun, Q. Adesope, S. C. Amagbor, T. D. Golden, F. D'Souza, T. R. Cundari, and J. A. Kelber, "Stability and activity of titanium oxynitride thin films for the electrocatalytic reduction of nitrogen to ammonia at different pH values." *Phys. Chem. Chem. Phys.*, **25**, 19540 (2023).
43. S. D. Young, B. M. Ceballos, A. Banerjee, R. Mukundan, G. Pilania, and B. R. Goldsmith, "Metal oxynitrides for the electrocatalytic reduction of nitrogen to ammonia." *J. Phys. Chem. C*, **126**, 12980 (2022).
44. C. E. Nanayakkara, P. M. Jayaweera, G. Rubasinghege, J. Baltrusaitis, and V. H. Grassian, "Surface photochemistry of adsorbed nitrate: the role of adsorbed water in the formation of reduced nitrogen species on α-Fe_2O_3 particle surfaces." *J. Phys. Chem.*, **118**, 158 (2014).
45. J. Baltrusaitis, P. M. Jayaweera, and V. H. Grassian, "XPS study of nitrogen dioxide adsorption on metal oxide particle surfaces under different environmental conditions." *Phys. Chem. Chem. Phys.*, **11**, 8295 (2009).
46. M. Lee, X. Ding, S. Banerjee, F. Krause, V. Smirnov, O. Astakhov, T. Merdzhanova, B. Klingebiel, T. Kirchartz, and F. Finger, "Bifunctional $CoFeVO_x$ catalyst for solar water splitting by using multijunction and heterojunction silicon solar cells." *Adv. Mater. Technol.*, **5**, 2000592 (2020).
47. X. Yang, J. Nash, J. Anibal, M. Dunwell, S. Kattel, E. Stavitski, K. Attenkofer, J. G. Chen, Y. Yan, and B. Xu, "Mechanistic insights into electrochemical nitrogen reduction reaction on vanadium nitride nanoparticles." *J. Am. Chem. Soc.*, **140**, 13387 (2018).
48. A. Osonkie, V. Lee, P. Chukwunenye, T. Cundari, and J. Kelber, "Plasma modification of vanadium oxynitride surfaces: Characterization by in situ XPS experiments and DFT calculations." *J. Chem. Phys.*, **153**, 144709 (2020).
49. O. Q. Carvalho, R. Marks, H. K. Nguyen, M. E. Vitale-Sullivan, S. C. Martinez, L. Árnadóttir, and K. A. Stoerzinger, "Role of electronic structure on nitrate reduction to ammonium: a periodic journey." *J. Am. Chem. Soc.*, **144**, 14809 (2022).